JOURNAL OF GEOPHYSICAL RESEARCH, VOL. 99, NO. C5, PAGES 10,035–10,048, MAY 15, 1994

Nonlinear wave interactions and high-frequency seafloor pressure

T. H. C. Herbers[1] and R. T. Guza

Center for Coastal Studies, Scripps Institution of Oceanography, La Jolla, California

Abstract. Linear wave theory predicts that pressure fluctuations induced by wind-generated surface gravity waves are maximum at the ocean surface and strongly attenuated at depths exceeding a horizontal wavelength. Although pressure fluctuations observed at the seafloor in deep water are indeed relatively weak at wind-wave frequencies, the energy at double wind-wave frequencies is frequently much higher than predicted by applying linear wave theory to near-surface measurements. These double-frequency waves can in theory be excited by nonlinear interactions between two surface wave components of about equal frequency, traveling in nearly opposing directions. Observations from a large aperture, 24-element array of pressure sensors deployed in 13-m depth are presented that quantitatively support this generation mechanism. As in previous studies, dramatic increases in the spectral levels of seafloor pressure at double wind-wave frequencies (0.3–0.7 Hz) frequently occurred after a sudden veering in wind direction resulted in waves propagating obliquely to preexisting seas. The observed spectral levels and vector wavenumbers of these double-frequency pressure fluctuations agree well with predictions obtained by applying second-order nonlinear, finite depth wave theory (Hasselmann, 1962) to the observed directionally bimodal seas. High-frequency seafloor pressure spectral levels also increased in response to directionally narrower but more energetic seas generated by strong, steady or slowly rotating winds. Bispectral analysis suggests that these pressure fluctuations are generated by nonlinear mechanisms similar to the veering wind cases.

1. Introduction

In linear theory the fluctuating pressure field of surface gravity waves is strongly attenuated at depths exceeding a horizontal wavelength. However, pressure fluctuations with about double the frequencies of swell and sea are often much more energetic at the seafloor than predicted by linear theory and are generally believed to be a second-order nonlinear effect [e.g., *Miche*, 1944; *Longuet-Higgins and Ursell*, 1948; *Phillips*, 1960; *Hasselmann*, 1962]. The nonlinear interaction between two free (i.e., obeying the dispersion relation) surface waves with frequencies f_1 and f_2 and wavenumbers $\mathbf{k}_1$ and $\mathbf{k}_2$ excites a forced secondary wave with the sum frequency $f_1 + f_2$ and sum (vector) wavenumber $\mathbf{k}_1 + \mathbf{k}_2$. Thus two primary waves of approximately equal frequency ($f_1 \approx f_2$) traveling in nearly opposing directions ($\mathbf{k}_1 \approx -\mathbf{k}_2$) theoretically force a secondary wave with about double the frequency of the primary waves and a relatively small wavenumber. The weakly attenuated pressure field of these high-frequency, long-wavelength secondary waves can excite deep-sea microseisms [*Longuet-Higgins and Ursell*, 1948].

The generation of double-frequency pressure fluctuations and microseisms by nonlinear interactions of directionally opposing surface waves has been studied both theoretically [e.g., *Longuet-Higgins*, 1950; *Hasselmann*, 1963; *Brekhovskikh*, 1966; *Hughes*, 1976; *Kibblewhite and Wu*, 1989] (see *Kibblewhite and Wu* [1991] for a recent review) and experimentally [e.g., *Cooper and Longuet-Higgins*, 1951; *Haubrich et al.*, 1963; *Nichols*, 1981; *Kibblewhite and Ewans*, 1985; *Webb and Cox*, 1986; *Cox and Jacobs*, 1989]. A detailed quantitative verification of the nonlinear theory for seafloor pressure has not been reported owing to the difficulty of simultaneously measuring the directional spectrum of wind waves and the associated forced pressure field. Recently, *Herbers and Guza* [1991, 1992] showed that double-frequency pressure fluctuations observed at the seafloor in 13-m depth agree reasonably well with predictions based on second-order nonlinear theory [*Hasselmann*, 1962] and concurrent measurements of the directional properties of sea waves. However, the accuracy of these theoretical predictions was limited by the poor directional resolution of the small aperture (20 m × 20 m) array of seven pressure sensors.

In the present study, data from a large-aperture (250 m × 250 m) array of 24 pressure transducers deployed in 13-m depth are used to investigate in more detail the nonlinear excitation of high-frequency pressure fluctuations. In this water depth, free surface waves with frequencies less than 0.3 Hz are only weakly attenuated, but above about 0.35 Hz the water column acts as a filter for free waves and relatively low-energy, long-wavelength forced waves are dominant at the seafloor. For example, the pressure spectral levels of free waves with frequencies 0.2, 0.4, and 0.6 Hz (37.9-, 9.7-, and 4.3-m wavelengths, respectively) are reduced by factors of roughly 10^{-2}, 10^{-7}, and 10^{-16}, respectively, from the sea

[1]Now at Department of Oceanography, Naval Postgraduate School, Monterey, California.

Paper number 94JC00054.
0148-0227/94/94JC-00054$05.00

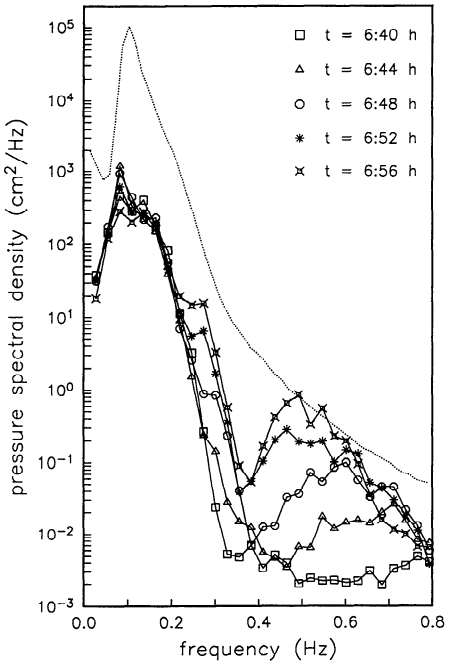

Figure 1. Large increases in spectral levels of seafloor pressure at double-wind-wave frequencies (about 0.35–0.7 Hz) frequently observed immediately following a sudden large shift in wind direction are illustrated with spectra (solid curves), collected at 4-min intervals (t = 6:40–6:56 hours in Figures 4a and 4b). Comparably energetic high-frequency pressure fluctuations (dotted curve) were generated by a strong, relatively steady wind (t = 39 hours in Figure 9a). The pressure spectral densities (here and elsewhere in this paper) have been converted to equivalent vertical water column displacements.

surface to the seafloor. There is about a factor 50 difference in the surface to bottom attenuation of pressure variance of 0.30- and 0.35-Hz free waves, the typical frequency range of very steep spectral roll-off with increasing frequency and of transition from free to forced waves (e.g., Figure 1) [see *Herbers and Guza*, 1991, 1992]. Thus both low-frequency ($f < 0.30$ Hz) wind-generated free waves and the corresponding long-wavelength portion of the high-frequency ($f > 0.35$ Hz) forced wave field can be measured at the seafloor. In addition to the interactions of directionally opposing waves with the same frequency that force double-frequency waves at the seafloor in deep water, seas with significantly different frequencies and/or propagation directions that deviate substantially from opposing are important to the forced bottom pressure field in finite water depth [e.g., *Herbers and Guza*, 1991]. Therefore the present observations are compared to a second-order finite depth theory [*Hasselmann*, 1962].

An overview of the field observations is given in section 2. The frequent and dramatic increases in double-frequency energy that occurred in response to large shifts in wind direction (an example is shown in Figure 1) are described in section 3. In section 4, spectral levels and wavenumbers of double-frequency seafloor pressure fluctuations observed during veering wind events are shown to be accurately predicted by second-order nonlinear theory [*Hasselmann*, 1962]. As discussed in section 5, spectral levels of high-frequency pressure fluctuations are elevated not only in response to a sudden shift in wind direction but also during strong steady winds and were maximum in a northeaster with directionally narrow but energetic seas (Figure 1). Bispectral analysis indicates that nonlinear surface wave interactions are also the source of these high-frequency seafloor pressure fluctuations. Although the present observations are generally consistent with theoretically predicted second-order nonlinear effects, it is shown in section 6 that third- and higher-order nonlinear effects are also detectable. The results are summarized in section 7.

2. Description of Observations

An array of 24 pressure transducers (250 m × 250 m aperture) was deployed on the seafloor in 13-m depth, 2 km offshore of Duck, North Carolina (Figure 2). The barrier island field site is exposed to sea waves with a wide range of local propagation directions [*Leffler et al.*, 1992, 1994]. The array geometry was tuned to the theoretically expected wavelengths of wind-generated seas and associated double-frequency secondary waves. Extensive surveys showed that uncertainties in sensor locations are less than 1% of the distance to the array center. To minimize flow noise, the

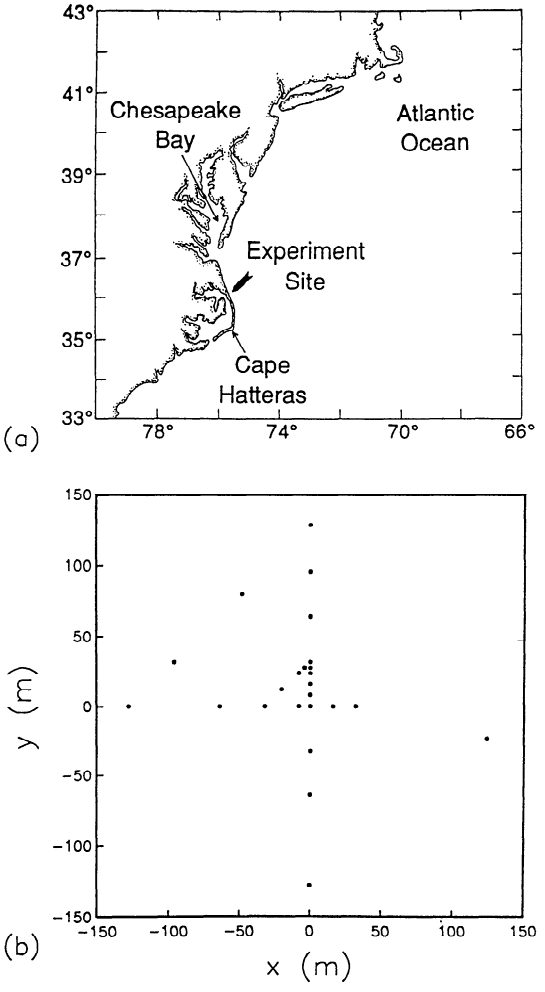

Figure 2. (a) Array location and (b) plan view: 24 pressure sensors (dots) were deployed on the seafloor in 13-m depth, 2 km offshore of Duck, North Carolina. The positive x-axis is directed offshore.

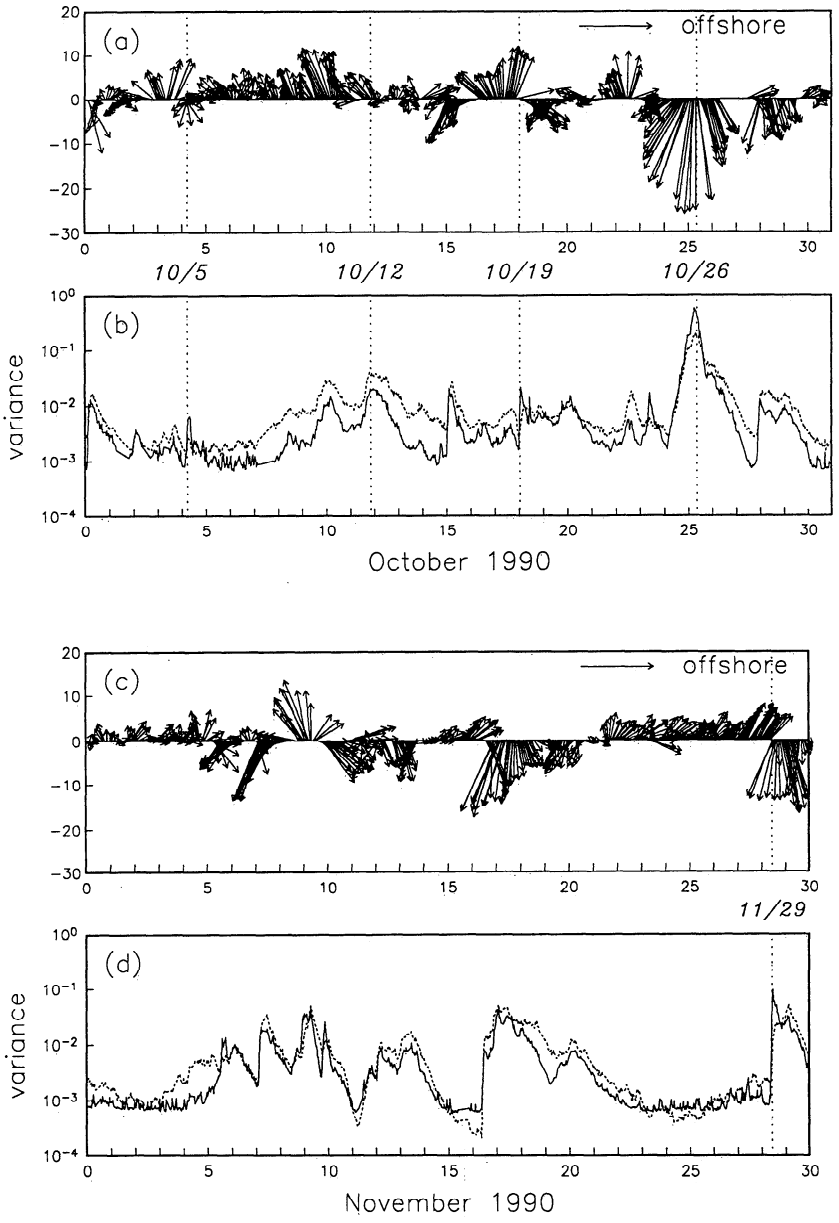

Figure 3. Hourly vector winds ((a) and (c) the y axis indicates the scale of the wind vectors in units of meters per second), surface wave variance (dashed curves in b and d units, of 10^5 cm^2), and pressure variance in the double-frequency range 0.35–0.70 Hz (solid curves in Figures 3b and 3d, units of cm^2) for (upper) October and (lower) November 1990. Wind measurements were collected on a nearby (within 1 km of the array site) pier. Surface wave variances were estimated from the seafloor pressure spectra in the frequency range 0.05–0.30 Hz based on the theoretical decay of free (linear) waves. The labeled vertical lines indicate events considered in detail.

transducers were buried about 10 cm within the sandy bottom [*Herbers and Guza*, 1991]. Data were collected at a 4-Hz sample rate between September 1990 and June 1991. The experiment is described in more detail by *Herbers et al.* [1994].

Throughout the 9 months of observations, the magnitude of pressure fluctuations at wind-wave and double wind-wave frequencies suddenly simultaneously increased during a rapid veering in wind direction, as illustrated in Figure 3 for October and November (when winds veered most frequently owing to the passage of weather fronts). Concurrent increases in microseism activity, similar to those reported by *Kibblewhite and Ewans* [1985], were observed in about 10-m depth within 1 km of the array site [*Yamamoto and Nye*, 1992]. Five case studies selected for further analysis, indicated by vertical lines on Figure 3, include both rapidly veering and relatively steady winds.

3. Seafloor Pressure Response to Veering Winds

The remarkably rapid response of seafloor pressure fluctuations at both sea and double-sea frequencies to a sudden shift in wind direction observed on November 29 (labeled 11/29 in Figures 3c and 3d) is detailed in Figures 1 and 4. The

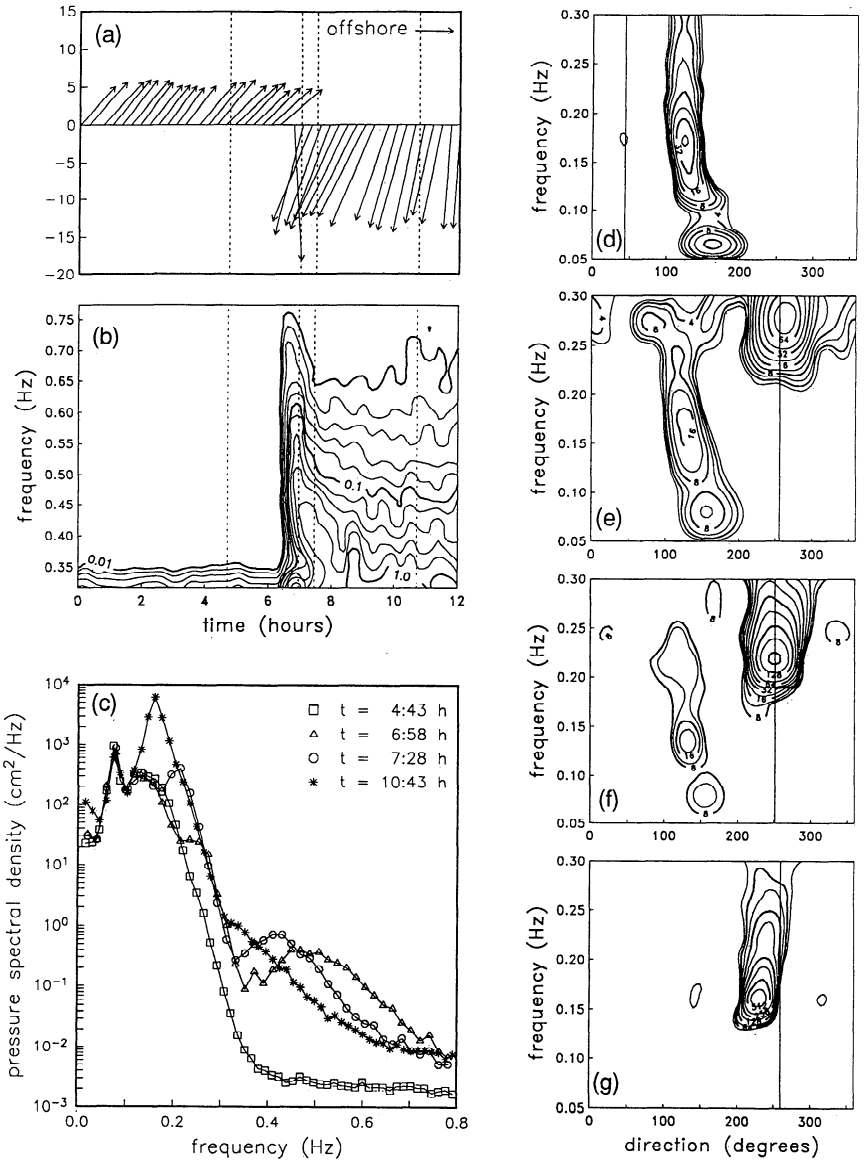

Figure 4. Response of surface waves and seafloor pressure to a rapidly veering wind. (a) History of 17-min average wind vectors (the y axis indicates the scale in units of meters per second). (b) History of double-frequency pressure spectral density (contours at $10^{0.2}$ intervals in units of cm^2/Hz) over the frequency range 0.3–0.8 Hz. (c) A sequence of frequency spectra of bottom pressure. (d)–(g) Corresponding sequence of frequency-directional spectra of sea surface elevation in the swell-sea frequency range 0.05–0.3 Hz (contours at $2^{0.5}$ intervals in units $cm^2/Hz°$), where $\theta = 180°$ is onshore propagation, and the vertical solid lines indicate the local wind direction. The times of the spectral estimates in Figures 4c–4g are indicated by vertical dashed lines in Figures 4a and 4b. The time origin ($t = 0$) is 03:25 hours, November 29, 1990.

double-frequency energy was maximum within an hour after the wind veered (Figures 4a and 4b), while the total surface wave energy continued to increase (Figures 3c and 3d). A sequence of four swell-sea frequency-directional spectra ($E_\eta(f, \theta)$, estimated from the array measurements using the variational technique described by *Herbers and Guza* [1990]) spanning this event is shown in Figures 4d–4g. Corresponding seafloor pressure frequency spectra ($E_p(f)$) are shown in Figure 4c.

Before the wind veered (t = 4:43 hours), the wave field is directionally narrow (Figures 4d) and double-sea-frequency energy is below the instrument noise level (approximately 2×10^{-3} cm^2/Hz in Figure 4c and 10^{-3} cm^2 in Figures 3b and 3d). Immediately after the wind veered (t = 6:58 hours), $E_\eta(f, \theta)$ is bimodal with a new 0.28-Hz sea peak (aligned with the new wind direction) directionally opposing preexisting seas (Figure 4e). The interaction of these seas results in a broad double-frequency peak in $E_p(f)$ centered at about 0.48 Hz (Figure 4c). At t = 7:28 hours, 1 hour after veering, the new wind-wave and double-frequency peaks have evolved to 0.22 Hz (Figure 4f) and 0.41 Hz (Figure 4c), respectively. The double-frequency energy has increased

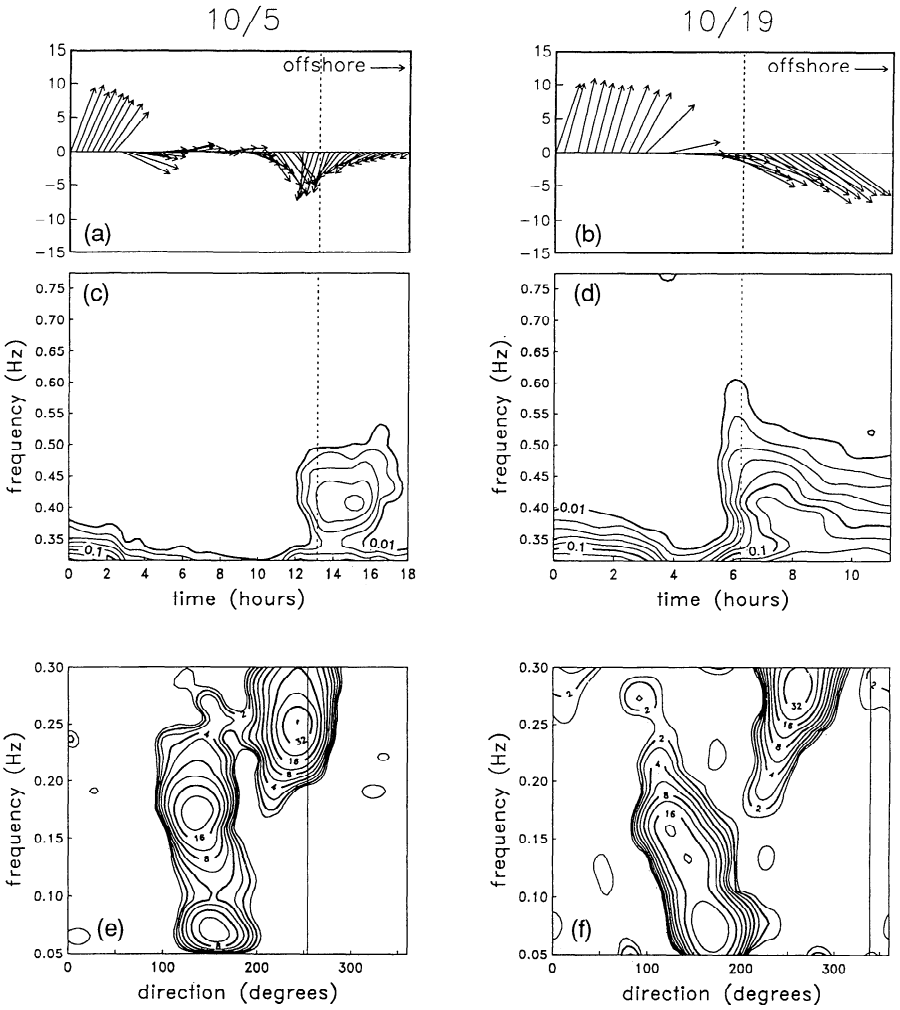

Figure 5. Veering winds, obliquely traveling seas, and double-frequency pressure fluctuations observed on (left) October 5 and (right) October 19. (a) and (b) History of 17-min average wind vectors. (c) and (d) History of double-frequency pressure spectral density. (e) and (f) Frequency-directional spectra of sea surface elevation at the times indicated by dashed vertical lines in Figures 5a–5d. The solid vertical lines indicate the local wind direction. Time origins (t = 0) are 16:25 hours, October 4, 1990 (Figures 5a and 5c) and 18:25 hours, October 18, 1990 (Figures 5b and 5d). Formats of the panels are the same as in Figure 4.

(relative to t = 6:58 hours) at frequencies below 0.45 Hz owing to interactions between the increasingly energetic new wind waves and the (only slowly decaying) residual waves opposing the wind (Figure 4f). At frequencies above about 0.25 Hz the waves opposing the wind have decayed (compare Figures 4e and 4f), resulting in a decrease in $E_p(f)$ above 0.5 Hz (Figure 4c). Four hours after the wind veered (t = 10:43 hours) the double-frequency peak in $E_p(f)$ has further downshifted and merged into the apparently saturated high-frequency shoulder of the 0.16-Hz sea peak (Figure 4c). The total surface wave energy has increased significantly, but pressure spectral levels above 0.4 Hz have decreased indicating that the energy levels of waves opposing the wind have decreased (Figure 4g). The sea propagation and local wind directions sometimes differed significantly (e.g., Figures 4d and 4g) owing to the limited fetch for offshore winds, refraction of low-frequency wind waves toward normal incidence to shore (θ = 180°), and perhaps spatial variability of the wind.

Two additional examples (October 5 and October 19, see Figure 3) of obliquely traveling wind waves generated by veering winds are shown in Figure 5 (corresponding $E_p(f)$ are shown in Figures 7a and 7b). Although the peaks in the directionally bimodal sea spectrum are only separated by about 100° on October 5, compared to ≈ 150° on October 19 and November 29, double-frequency pressure energy levels at the seafloor are still significantly elevated. In this intermediate depth (h = 13 m) water, interactions between all obliquely propagating (i.e., not necessarily opposing) wind-wave pairs with vector wavenumbers ($\mathbf{k}_1$, $\mathbf{k}_2$) such that $|\mathbf{k}_1 + \mathbf{k}_2|h \leq O(1)$ force weakly attenuated pressure fluctuations at the seafloor. The evolution shown in Figures 4 and 5 is typical of the many veering wind events examined, and similar to the general patterns of evolution observed by *Kibblewhite and Ewans* [1985].

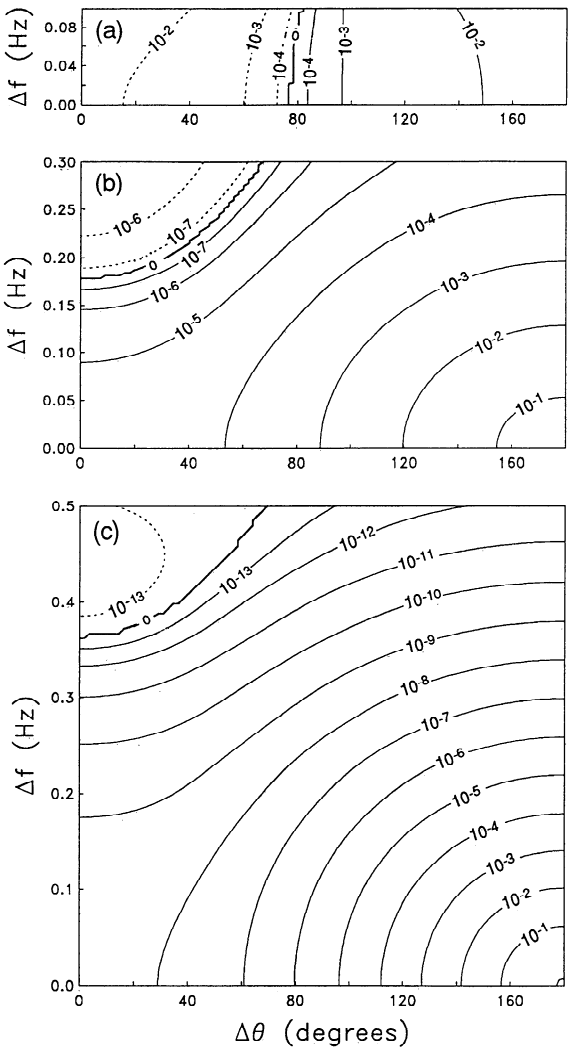

Figure 6. The coefficient $M(f/2 - \Delta f/2, f/2 + \Delta f/2, \Delta\theta)$ (units of m^{-2}) for the forcing of secondary seafloor pressure fluctuations with frequency f by the interaction of two surface waves with differences in frequency Δf and propagation direction $\Delta\theta$ (equation (2)), as a function of Δf and $\Delta\theta$ for f = (a) 0.2 Hz, (b) 0.4 Hz, and (c) 0.6 Hz. Solid and dashed contours indicate interactions for which the pressure bispectrum (Appendix B, equation (B1)) is negative and positive, respectively.

4. Comparison to Second-Order Nonlinear Wave Theory

Weakly nonlinear theories for surface gravity waves [*Miche*, 1944; *Longuet-Higgins and Ursell*, 1948; *Phillips*, 1960; *Hasselmann*, 1962] predict secondary pressure fluctuations owing to interactions of two wind-wave components. At great depth, only very long wavelength, double-frequency pressure fluctuations excited by directionally opposing waves of equal frequency are unattenuated, and compressibility effects are important [*Longuet-Higgins*, 1950; *Hasselmann*, 1963]. In the intermediate depth where the present observations were collected, compressibility effects are negligible [e.g., *Longuet-Higgins*, 1950] and a broader range of interactions drive seafloor pressure fluctuations.

Assuming an incompressible fluid on a rigid flat sea bed, the lowest-order sea surface is described by a frequency-directional spectrum $E_\eta(f, \theta)$ of free waves with wavenumbers $\mathbf{k} = [k \cos\theta, k \sin\theta]$ obeying the dispersion relation

$$2\pi f = [gk \tanh(kh)]^{1/2} \tag{1}$$

The spectrum of nonlinearly forced secondary seafloor pressure is (neglecting difference-frequency interactions)

$$E_{p,\text{forced}}(f) = \int_0^f d\Delta f \int_0^{2\pi} d\theta_1 \int_0^{2\pi} d\theta_2 \cdot M(f/2 - \Delta f/2, f/2 + \Delta f/2, |\theta_1 - \theta_2|) \cdot E_\eta(f/2 - \Delta f/2, \theta_1) E_\eta(f/2 + \Delta f/2, \theta_2) \tag{2}$$

where the interaction coefficient M is a complicated function of the differences in frequency (Δf) and propagation direction ($\Delta\theta = |\theta_1 - \theta_2|$) of the interacting free waves [*Hasselmann*, 1962; *Hasselmann et al.*, 1963]. Regions of Δf, $\Delta\theta$ space where M is large contribute most efficiently to the forced seafloor pressure field.

The dependence of M on Δf and $\Delta\theta$ in 13-m depth for frequencies f = 0.2, 0.4, and 0.6 Hz is shown in Figure 6 (see also *Herbers and Guza* [1991]). For f = 0.4 and 0.6 Hz, M is maximum for free waves of equal frequency (Δf = 0) traveling in opposing directions ($\Delta\theta$ = 180°). For f = 0.6 Hz (Figure 6c), M is reduced by more than a factor 10^{-5} for either $\Delta\theta < 90°$ or $\Delta f > 0.2$ Hz. For f = 0.4 Hz (Figure 6b), the dependence of M on Δf and $\Delta\theta$ is weaker; the reduction for the same $\Delta\theta$ (90°) or Δf (0.2 Hz) is only about a factor 10^{-2}–10^{-3}. Thus 0.6-Hz seafloor pressure fluctuations are excited primarily by nearly directionally opposing waves of about equal frequency (0.3 Hz) whereas the seafloor pressure field at 0.4 Hz can result from a broader range of interactions. At 0.2 Hz, values of M for colinear ($\Delta\theta$ = 0) and opposing ($\Delta\theta$ = 180°) wave interactions are about equal, so that the forced pressure field is likely to be dominated by small $\Delta\theta$ interactions owing to the typically small amounts of directionally opposing energy. Furthermore, free wind waves at 0.2 Hz are not strongly attenuated in 13-m depth and the bottom pressure spectrum usually contains a mix of free and forced waves [e.g., *Herbers et al.*, 1992].

Theoretically predicted spectra of forced secondary pressure fluctuations ($E_{p,\text{forced}}(f)$) in the frequency range 0.3–0.5 Hz are compared to observed spectra ($E_p(f)$) in Figures 7a–7c for three occasions (Figures 4 and 5) when veering winds generated obliquely traveling seas and elevated double-frequency energy. The predictions were obtained by substituting in (2) the $E_\eta(f, \theta)$ estimates in the swell-sea frequency range 0.05–0.3 Hz (Figures 4e, 5e, and 5f). Also shown are comparisons of observed and predicted root-mean-square wavenumbers $k_{\text{rms}}(f)$ (Figures 7d–7f)

$$k_{\text{rms}}(f) \equiv \left[\frac{\int_0^{k_c} dk \int_0^{2\pi} k\, d\theta\, k^2 E_p(f, k, \theta)}{\int_0^{k_c} dk \int_0^{2\pi} k\, d\theta\, E_p(f, k, \theta)} \right]^{1/2} \tag{3}$$

and vector-averaged mean propagation directions $\theta_{\text{mean}}(f)$ (Figures 7g–7i)

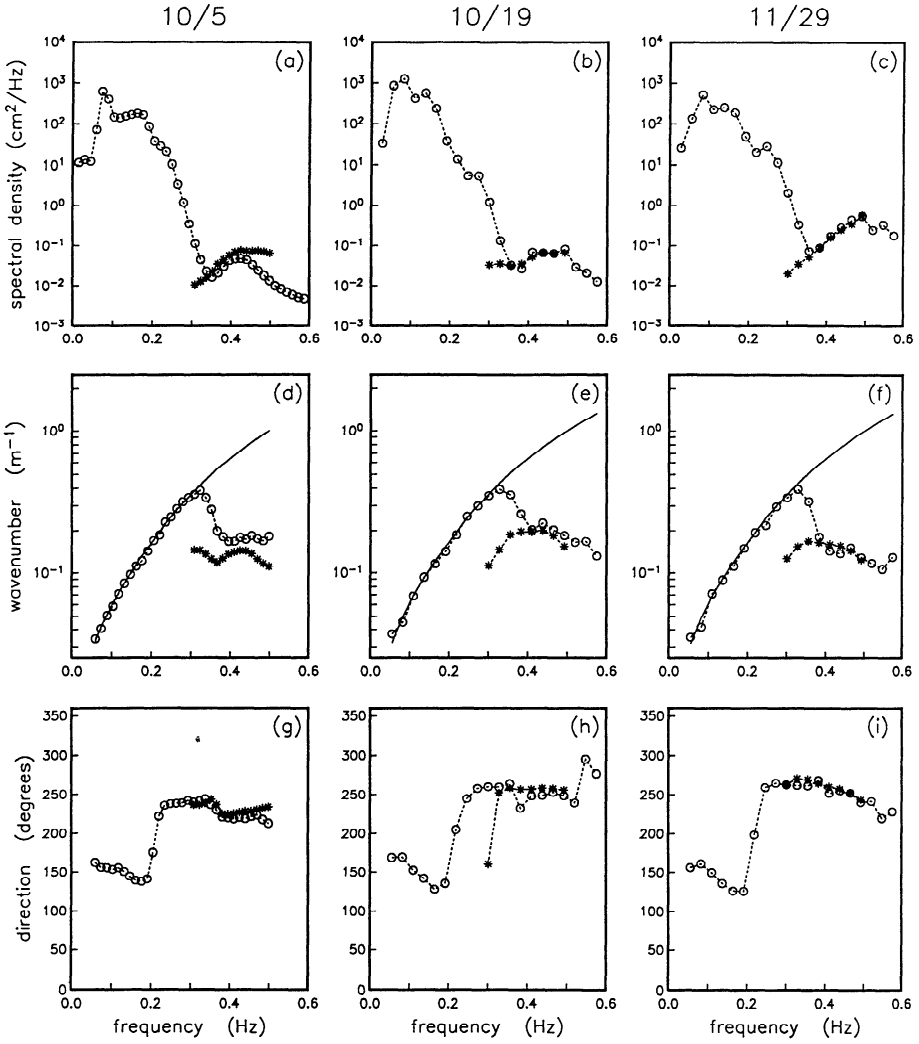

Figure 7. Comparison of observed (open circles) and predicted (asterisks; in the frequency range 0.3–0.5 Hz) seafloor pressure fluctuations. (a)–(c) Pressure frequency spectra $E_p(f)$. (d)–(f) Average wavenumber magnitudes $k_{\text{rms}}(f)$ (equation (3)), the solid curve is the linear dispersion relation (equation (1)). (g)–(i) Mean propagation directions $\theta_{\text{mean}}(f)$ (equation (4)). Results are shown for (left) October 5, (center) October 19, and (right) November 29, corresponding to the swell-sea frequency-directional spectra in Figures 5e, 5f, and 4e, respectively. Estimates of k_{rms} and θ_{mean} are shown only for frequencies where E_p is well above the instrument noise floor.

$$\tan\left[\theta_{\text{mean}}(f)\right] \equiv \frac{\int_0^{k_c} dk \int_0^{2\pi} k\, d\theta\, k \sin\theta E_p(f, k, \theta)}{\int_0^{k_c} dk \int_0^{2\pi} k\, d\theta\, k \cos\theta E_p(f, k, \theta)} \tag{4}$$

where $E_p(f, k, \theta)$ is the frequency (vector) wavenumber spectrum of seafloor pressure. Contributions to $E_p(f, k, \theta)$ at wavenumbers larger than the cutoff wavenumber $k_c \approx 2\pi/h$ are expected to be negligible owing to the exponential vertical decay of waves with wavelengths less than the water depth [e.g., *Herbers and Guza*, 1992]. The method used to estimate $k_{\text{rms}}(f)$ and $\theta_{\text{mean}}(f)$ from the array data is briefly described in Appendix A. Equations with a structure similar to (2) yield theoretical predictions of $k_{\text{rms}}(f)$ and $\theta_{\text{mean}}(f)$ at double wind-wave frequencies [*Herbers and Guza*, 1992].

The observed and predicted forced wave energy levels, wavenumbers, and propagation directions are generally in good agreement over the frequency range 0.35–0.5 Hz (Figures 7). The comparisons are restricted to this narrow-frequency range as a consequence of using the same array to observe both free and forced waves. Since forced waves dominate the seafloor pressure measurements above 0.35 Hz, the directional properties of high-frequency (>0.3 Hz) wind waves are not available, and accurate forced wave predictions are limited to frequencies less than about 0.5 Hz [*Herbers and Guza*, 1991]. At frequencies below 0.35 Hz the observed motions are a mix of free and forced waves but the predictions account only for forced waves. The observed k_{rms} (Figures 7d–7f) are very close to the linear wave dispersion relation (equation (1)) at frequencies below 0.3 Hz, consistent with the hypothesis that free waves dominate the pressure field below 0.3 Hz. Above about 0.35 Hz, the

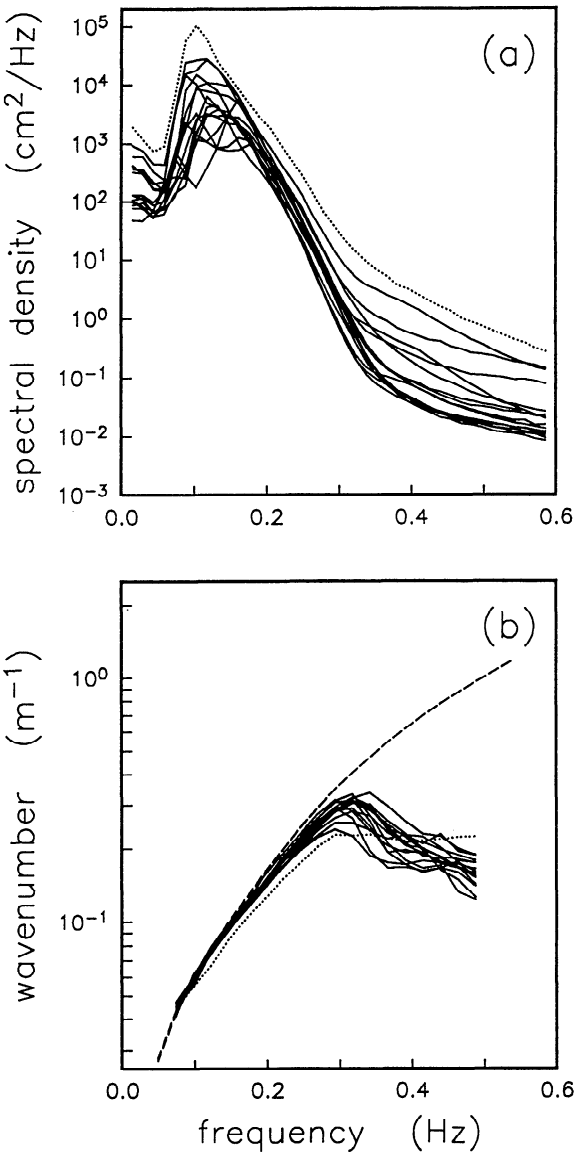

Figure 8. (a) Frequency spectra $E_p(f)$ and (b) root-mean-square wavenumbers $k_{rms}(f)$ of seafloor pressure observed during steady winds. Dotted curves are estimates during a northeaster on October 26 (t = 39 hours in Figure 9), when the wind speed, sea energy, and high-frequency pressure levels were maximum. The dashed curve in Figure 8b denotes the linear dispersion relation.

attenuation of free waves and dominance of longer-wavelength forced waves cause the observed and predicted k_{rms} to deviate from the linear dispersion curve.

The observed and predicted double-frequency wave fields are in better overall agreement than similar comparisons using a much smaller array of pressure sensors [*Herbers and Guza*, 1991, 1992]. The somewhat larger discrepancies observed on October 5 above 0.4 Hz (Figures 7a and 7d), compared to October 19 (Figures 7b and 7e) and November 29 (Figures 7c and 7f), may be owing to errors in the predictions caused by small inaccuracies in the $E_\eta(f, \theta)$ estimate. On this occasion the directional separation between the two sea peaks is only about 100° (Figure 5e, compared to about 150° in Figures 4e and 5f). Since the value of M for 0.4-Hz forced waves excited by $\Delta\theta = 100°$ interactions is about a factor 10^{-2} smaller than the maximum value of M for $\Delta\theta = 180°$ (Figure 6b), a weak sidelobe in the $E_\eta(f, \theta)$ estimate at an angle opposing the dominant seas can contribute a relatively large error in the forced wave prediction. This sensitivity increases with increasing forced wave frequency (e.g., the same reduction of M for 0.6-Hz forced waves is about 10^{-5}, Figure 6c). Thus the differences between predictions and observations are plausibly explained by the limitations of the array data and do not suggest a violation of the assumptions used in second-order nonlinear wave theory or the presence of high-frequency pressure fluctuations driven by other mechanisms. The present observations are quantitatively consistent with the theory that double-frequency energy peaks following a rapid veering in wind direction result from nonlinear interactions between obliquely traveling wind waves and that these forced pressure fluctuations have the sum (vector) wavenumber of the interacting waves.

5. Seafloor Pressure Response to Steady Winds

Pressure spectral levels at double wind-wave frequencies were also observed to be elevated during periods of strong, steady winds. For example, after the November 29 veering wind event, the double-frequency energy levels do not relax back to the low pre-veering values but remain elevated, presumably in response to a steady alongshore wind (Figures 4a and 4b). Pressure spectra observed during 16 randomly selected episodes of relatively steady, moderate to strong winds are featureless at high frequencies (Figure 8a), lacking the distinct double-frequency peak characteristic of veering wind events (e.g., Figure 4c). However, qualitatively similar to wavenumbers observed during veering wind events (Figures 7d–7f), the $k_{rms}(f)$ estimates in steady winds (Figure 8b) transition from free wave values at frequencies below 0.3 Hz to longer wavelengths at higher frequencies.

The strongest winds and maximum sea energy levels during the 9 months of observations occurred in a severe northeaster storm (Figure 1, labeled 10/26 in Figures 3a and 3b). During a 30-hour period the wind slowly rotated from onshore to alongshore, and increased in mean speed from less than 5 to 25 m/s (Figure 9a), with gusts exceeding 40 m/s. This event was examined in more detail because the high-frequency pressure spectral levels exceeded the levels observed in veering wind events (Figure 1) but also because the intense wave breaking at the array (the maximum significant wave height was about 4 m) raises the possibility that turbulence contributed significantly to the bottom pressure field.

Whereas the frequency-directional surface wave spectra $E_\eta(f, \theta)$ generated by veering winds are typically bimodal with obliquely traveling preexisting and new seas (e.g., Figures 4e, 4f, 5e, and 5f), the $E_\eta(f, \theta)$ observed in steady or slowly rotating winds are usually unimodal with most of the energy contained within ±45° of the spectral peak direction (e.g., Figure 4g). Existing measurements, including the spatially extensive many-element array data used in the present study, fundamentally lack the resolution to detect relatively low energy waves traveling at large oblique angles in steady winds. Parameterizations of $E_\eta(f, \theta)$ based on such observations [e.g., *Longuet-Higgins et al.*, 1963; *Tyler et al.*, 1974; *Mitsuyasu et al.*, 1975; *Hasselmann et al.*, 1973,

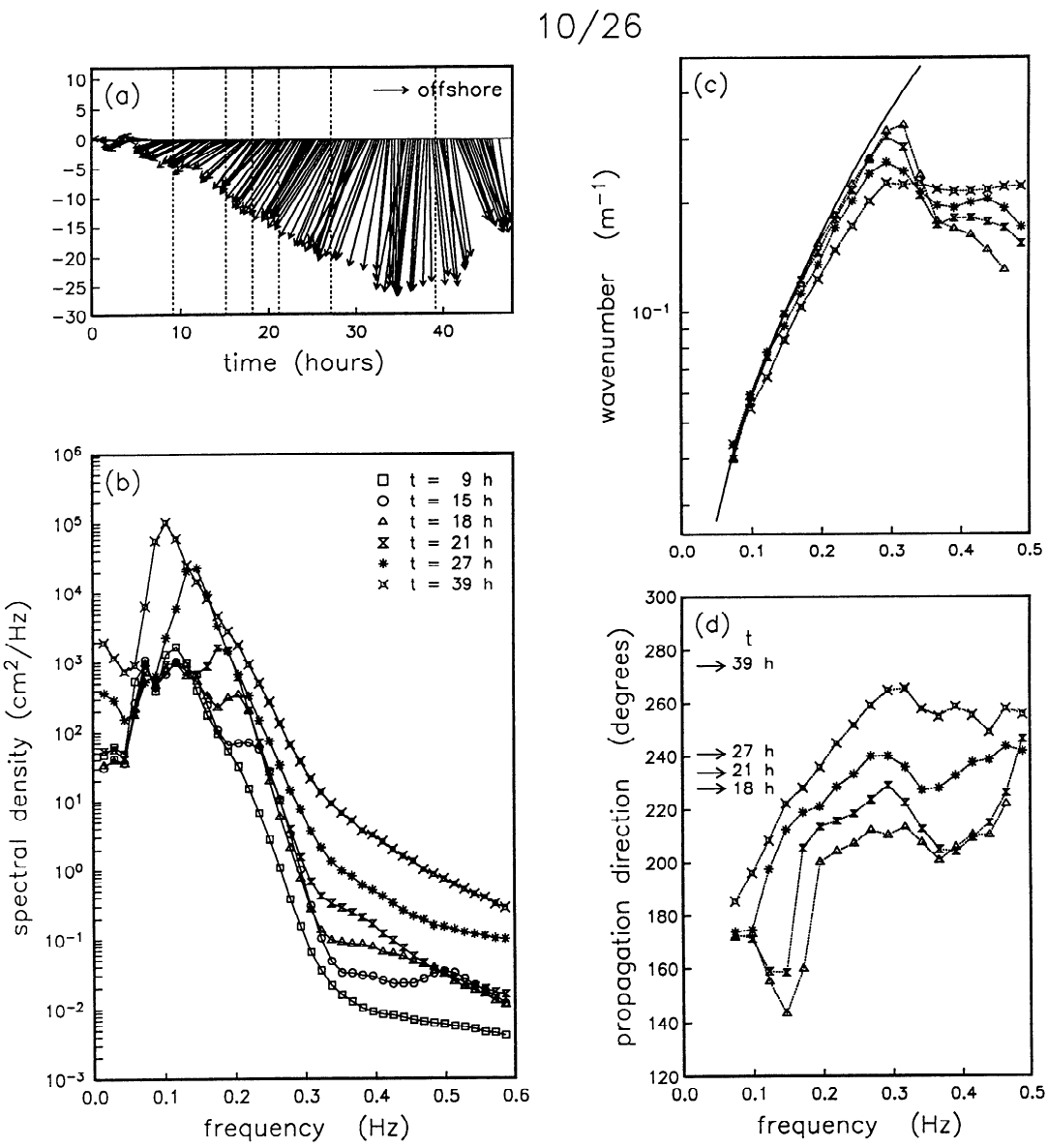

Figure 9. Response of surface waves and seafloor pressure to a strong and slowly rotating wind. (a) History of 17-min average wind vectors (same format as Figure 4a). (b) Sequence of bottom pressure frequency spectra. (c) Estimates of $k_{rms}(f)$ corresponding to the last four spectra in Figure 9b. The solid curve is the dispersion relation for linear waves. (d) Estimates of $\theta_{mean}(f)$ corresponding to the last four spectra in Figure 9b. Arrows show the local wind direction (180° is onshore) at the indicated times. Times of the estimates in Figures 9b–9d are indicated by vertical dashed lines in Figure 9a. The time origin (t = 0) is 17:17 hours, October 24, 1990.

1980; *Donelan et al.*, 1985] thus do not accurately describe the tails of directional wind-wave energy distributions. The energy levels of waves opposing steady winds, which strongly influence double-frequency pressure spectral levels at the seafloor, are unknown.

Because of the sensitivity of predictions to the unresolvable waves propagating at large oblique angles relative to the wind, detailed comparisons to second-order theory (e.g., Figure 7) are not presented in the following analysis of cases with steady or slowly rotating winds. Instead, bispectral analysis is used to test the hypothesis that the observed high-frequency pressure fluctuations result from nonlinear wind-wave interactions. The bispectrum $B(f_1, f_2)$ (Appendix B), normalized by the spectral densities at frequencies f_1, f_2 and $f_1 + f_2$

$$b(f_1, f_2) \equiv \frac{B(f_1, f_2)}{[E(f_1)E(f_2)E(f_1 + f_2)]^{1/2}} \quad (5)$$

detects nonlinear phase coupling between wave components with frequencies f_1, f_2, and $f_1 + f_2$ [e.g., *Hasselmann et al.*, 1963; *Haubrich*, 1965; *Masuda and Kuo*, 1981; *Elgar and Guza*, 1985; *Herbers and Guza*, 1992].

The real part of $b(f_1, f_2)$ is shown in Figure 10 at 4 times during the October 26 northeaster. As predicted theoretically [*Hasselmann et al.*, 1963], the imaginary part is ap-

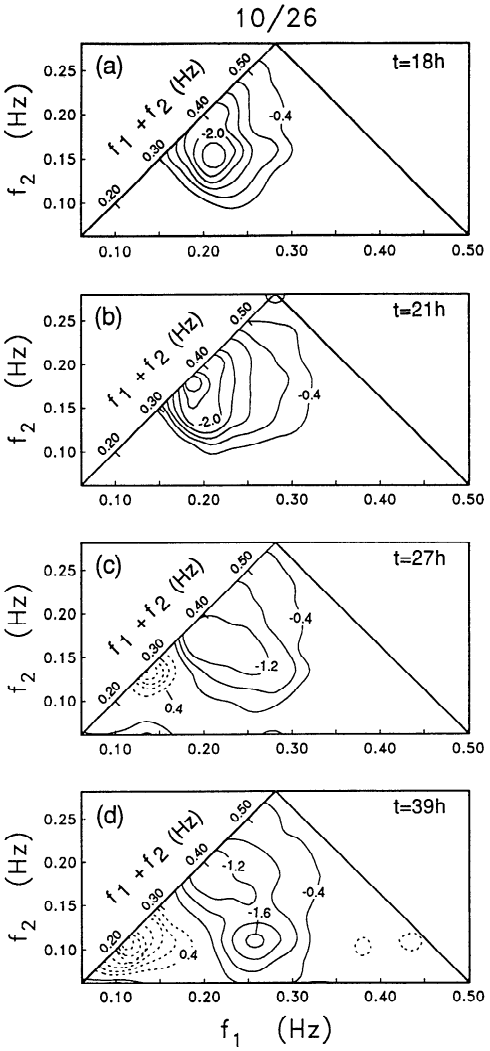

Figure 10. Evolution of the real part of the normalized bispectrum $b(f_1, f_2)$ (equation (5); units of $Hz^{-1/2}$, contour interval 0.4 $Hz^{-1/2}$) during the October 26 northeaster. Times of the estimates are indicated by the last four vertical lines in Figure 9a. Corresponding spectra, wavenumbers, and propagation directions are shown in Figures 9b–9d. Solid and dashed contours denote negative and positive values, respectively. Nonzero values indicate nonlinear phase coupling between waves with frequencies f_1, f_2, and $f_1 + f_2$.

proximately randomly scattered about zero (Figure 11). The negative sign of the broad peak in the bispectrum at $f_1 \approx 0.22$ Hz, $f_2 \approx 0.15$ Hz during the initial phase of the storm ($t = 18$ hours, Figure 10a) is theoretically expected (Figure 6b) for pressure fluctuations forced by the interaction between new 0.22-Hz seas and obliquely traveling ($\Delta\theta \approx 70°$, Figure 9d) preexisting 0.15-Hz seas. Three hours later the new sea peak is more energetic and shifted to about 0.18 Hz (Figure 9b, $t = 21$ hours). The peak in the bispectrum has shifted to $f_1 \approx f_2 \approx 0.18$ Hz (Figure 10b), suggesting that the dominant interactions no longer involve preexisting seas but are between more energetic new seas. At $t = 27$ hours the energy of the sea peak has increased dramatically and downshifted to about 0.14 Hz (Figure 9b). The corresponding peak in the bispectrum at $f_1 \approx f_2 \approx 0.14$ Hz is positive (Figure 10c), consistent with the theoretical phase relationship for colinearly forced secondary waves (Figure 6a, $\Delta\theta \approx 0$). Colinear interactions are expected to dominate the forced pressure field below about 0.3 Hz unless the directional wind-wave spectrum is extremely broad (Figure 6a). At higher sum frequencies, $b(f_1, f_2)$ remains negative (Figure 10c) consistent with the expected forcing by interactions of obliquely traveling waves (Figure 6b).

At the height of the storm ($t = 39$ hours, Figure 9b) the spectral peak has further downshifted to about 0.1 Hz, and the positive peak in the bispectrum, corresponding to colinear interactions of the dominant seas, is similarly downshifted (Figure 10d). Between $t = 18$ hours and $t = 39$ hours the k_{rms} estimates in Figure 9c show increasingly large deviations from the linear dispersion curve in the frequency range 0.2–0.3 Hz, consistent with the transition from free wave (Figures 10a and 10b) to forced wave (Figures 10c and 10d) dominance observed in the bispectral estimates. At higher sum frequencies the negative sign of the bispectrum indicates the dominance of interactions between obliquely traveling waves similar to earlier stages of the storm (Figures 10a–10c). However, in addition to the expected $f_1 \approx f_2$ ridge of interactions between waves of nearly equal frequency, there is a broad negative peak centered at $f_1 \approx 0.26$ Hz, $f_2 \approx 0.11$ Hz. A plausible explanation for this peak is interactions between the dominant 0.1-Hz waves traveling approximately normal to shore (180°) and locally generated waves aligned with the alongshore (270°) wind (Figure 9d). The contributions of these relatively short wavelength forced waves may be significant because of the very high energy levels at frequencies near the spectral peak (eq. 2), even though the interaction coefficient M for $\Delta\theta = 90°$ and $\Delta f = 0.15$ Hz is about a factor 10^3 smaller than the maximum M for $\Delta\theta = 180°$, $\Delta f = 0$ (Figure 6b). The k_{rms} at high frequencies (>0.35 Hz) are maximum at the height of the northeaster ($t = 39$ hours, Figure 9c), qualitatively consistent with contributions of large Δf (and hence large $|\mathbf{k}_1 + \mathbf{k}_2|$) interactions between the energetic spectral peak and local seas.

6. Discussion

Although the bispectra and wavenumber estimates for the October 26 northeaster (Figures 9–11) and other occasions of steady or slowly rotating winds (Figure 8, bispectra not shown) are qualitatively consistent with second-order nonlinear theory, it is possible that third- and higher-order forced waves contribute significantly to the high-frequency bottom pressure field. For example, at the height of the northeaster the negative bispectral values observed at $f_1 \approx 0.26$ Hz, $f_2 \approx 0.11$ Hz (Figure 10d) are plausibly explained

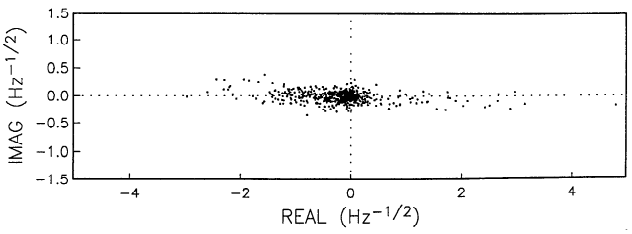

Figure 11. Imaginary versus real parts of the bispectra shown in Figures 10 and 12.

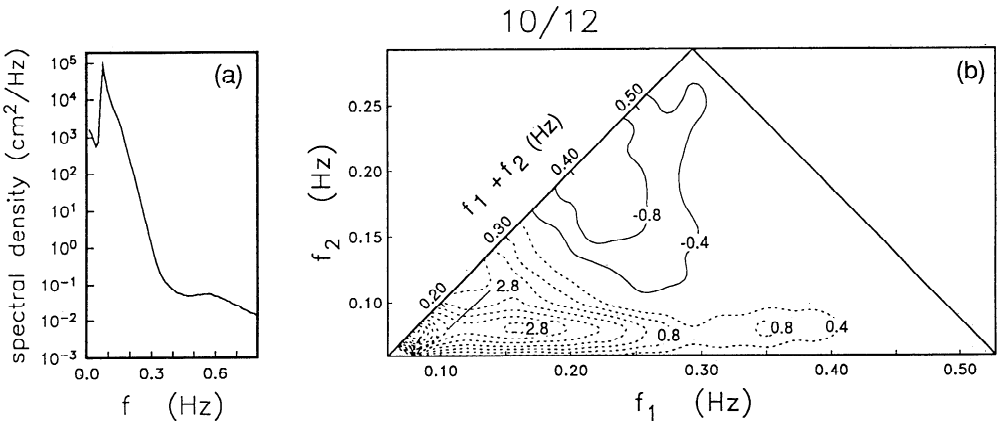

Figure 12. (a) Seafloor pressure spectrum and (b) bispectrum (same format as Figure 10) observed on October 12, 1990, 20:25 hours, during the arrival of energetic swell (the significant wave height was about 2.5 m) from a distant hurricane.

by second-order interactions of obliquely traveling waves, but at these relatively high sum frequencies ($f_1 + f_2$ is 3–4 times the spectral peak frequency), contributions of tertiary and quartenary forced waves could also be important.

As discussed by *Kibblewhite and Wu* [1991], both second- and higher-order nonlinear interactions can drive unattenuated pressure fluctuations. In general, the nonlinear interaction between N surface wave components with wavenumbers ($\mathbf{k}_1, \mathbf{k}_2, \cdots, \mathbf{k}_N$) and frequencies ($f_1, f_2, \cdots, f_N$) (given by the dispersion relation, equation (1)) yields a forced wave component with the sum frequency ($f_1 + f_2 + \cdots + f_N$) and wavenumber ($\mathbf{k}_1 + \mathbf{k}_2 + \cdots + \mathbf{k}_N$) that reaches the seafloor if $|\mathbf{k}_1 + \mathbf{k}_2 + \cdots + \mathbf{k}_N|h \leq O(1)$. An example is the interaction between two swell components with about equal frequencies (f_{swell}) and propagation directions (θ_{swell}) and a higher-frequency ($f_{\text{sea}} > f_{\text{swell}}$), directionally opposing ($\theta_{\text{sea}} = \theta_{\text{swell}} + \pi$) sea component. In deep water the condition that the resulting forced tertiary wave with frequency $2f_{\text{swell}} + f_{\text{sea}}$ reaches the seafloor is satisfied for $f_{\text{sea}} = 2^{1/2} f_{\text{swell}}$.

In the present data set, higher-order nonlinear interactions are detectable during the arrival of energetic 0.07-Hz swell from a distant hurricane (Figure 12). The negative $b(f_1, f_2)$ values for $f_1 + f_2 > 0.3$ Hz are characteristic of second-order interactions between obliquely traveling seas (e.g., Figure 10). However, the ridge of positive values for constant $f_2 \approx 0.07$ Hz, extending to sum frequencies as high as 0.5 Hz, may be caused by higher-order interactions between energetic swell components (Appendix B). Since the primary swell is in relatively shallow water ($kh \approx 0.5$), forced colinear harmonic waves approximately obey the shallow water dispersion relation $k = (2\pi f)/(gh)^{1/2}$ and can reach the seafloor even for frequencies as high as 0.5 Hz. For example, in 13-m depth the spectral decay at the seafloor of 0.5-Hz high-order forced waves obeying the shallow water dispersion relation is 3×10^{-3}, compared to a decay of 8×10^{-6} for 0.5-Hz secondary waves forced by colinear 0.25-Hz primary waves, and 2×10^{-11} for 0.5-Hz free waves. During the northeaster, similar higher-order colinear forced waves were presumably excited but not detected because they were submerged in more energetic high-frequency pressure fluctuations driven by interactions between obliquely traveling seas (Figure 10d). During the arrival of hurricane swell, local winds were light and sea energy levels low, exposing higher-order swell interactions (Figure 12).

Although the theory for the tertiary forced wave field generated by a frequency-directional spectrum of surface waves has been developed [*Hasselmann*, 1962], the consequences of these and higher-order nonlinear interactions to the seafloor pressure field has not been further explored. Similar to second-order forced waves, the weakly attenuated higher-order forced wave field is probably a strong function of $E_\eta(f, \theta)$, and higher-order spectral analysis techniques are needed to identify the interacting wave components.

Theory predicts that microseisms are generated only by seafloor pressure fluctuations with the same phase velocity as a freely propagating seismic wave [e.g., *Hasselmann*, 1963]. Although the observed root-mean-square average wavenumbers k_{rms} of forced high-frequency pressure fluctuations are much less than the wavenumbers of free surface gravity waves obeying the linear dispersion relation (Figures 7d–7f, 8b, and 9c), the k_{rms} are still several orders of magnitude larger than the typical wavenumbers predicted for microseisms. On shallow continental shelves a broad range of interactions drive weakly attenuated pressure fluctuations, but only the very long-wavelength components in this pressure field can excite microseisms. No attempt was made to estimate the spectral levels of the source pressure field for microseisms from the present observations, because the array aperture is too small and the record lengths (limited by the duration of stationary wind-wave fields) too short to adequately resolve the propagation of these relatively weak long-wavelength components in a background of shorter-wavelength forced waves.

7. Summary

The generation of pressure fluctuations at the seafloor in the frequency range 0.3–0.7 Hz, about double the frequencies of wind-generated seas, is investigated with data from a 24-element array of pressure sensors, deployed in 13-m depth on the North Carolina shelf (Figure 2). In this depth, swell and sea components (frequencies in the range 0.05–0.3 Hz) are only weakly attenuated at the seafloor, but free surface waves with frequencies higher than 0.35 Hz have wavelengths less than the water depth and are strongly

attenuated. Above 0.35 Hz, the seafloor pressure spectrum is dominated by long-wavelength, weakly attenuated pressure fluctuations that are forced by nonlinear interactions between pairs of surface wave components traveling at oblique angles.

Dramatic increases in seafloor pressure spectral levels at double the frequencies of locally generated seas were frequently observed following a rapid veering in local wind direction (Figure 3). Frequency-directional spectra $E_\eta(f, \theta)$ of wind waves (estimated from the array data) are typically narrow both prior to (Figure 4d) and well after the wind shift (Figure 4g). Immediately after the wind shift, $E_\eta(f, \theta)$ is bimodal with obliquely traveling new and preexisting seas (Figures 4e, 5e, and 5f), and a double-sea-frequency peak develops (Figures 4a, 4b, and 5a–5d). Both the new sea peak and the double-frequency peak rapidly increase in energy (sometimes by a factor of 10^2–10^3 in less than 20 min, Figure 1). The preexisting seas gradually decay (Figure 4f), and the double-frequency peak shifts to lower frequencies, eventually merging into the high-frequency tail of the fully developed new sea spectrum (Figure 4c).

The observed double-frequency pressure fluctuations are compared to predictions based on second-order nonlinear theory and the observed directionally bimodal seas. The good agreement between observed and predicted energy levels, wavenumber magnitudes, and propagation directions (Figure 7) adds confidence to the conclusion of *Herbers and Guza* [1991, 1992, and references therein] that the double-frequency seafloor pressure fluctuations are forced secondary waves excited by nonlinear interactions between obliquely traveling surface waves.

Pressure spectral levels at double-wind-wave frequencies increase both after a sudden shift in wind direction and in response to strong, relatively steady winds. During the 9-month experiment the highest-energy levels in the frequency range 0.3–0.7 Hz occurred in a northeaster when both the wind speed and surface wave energy were maximum (Figure 1). The evolution of the pressure field during this storm was quite different from the response to veering winds (compare Figures 4a and 4c with Figures 9a and 9b). After a sudden shift in wind direction the rapid (timescales of minutes) increase in double-frequency pressure spectral levels is followed by a gradual decay. The sea energy continues to increase, but the directional distribution narrows and nonlinear forcing of long-wavelength, high-frequency waves is less efficient. In contrast, during slowly rotating winds, double-frequency energy levels increase slowly (timescales of hours-days) and are maximum when the sea energy is maximum. The directional distribution of sea energy remains relatively narrow and increases in double-frequency energy result primarily from increases in sea energy. Wavenumbers (Figures 8b and 9c) and bispectra (Figures 10 and 11) observed in steady or slowly rotating winds are qualitatively consistent with the generation of long-wavelength, high-frequency seafloor pressure fluctuations by nonlinear interactions of obliquely traveling waves.

Bispectra observed during the arrival of energetic low-frequency swell, when local sea energy levels were low, are consistent with the generation of high-frequency pressure fluctuations by third- and higher-order nonlinear interactions between the dominant swell components (Figure 12). Further work is needed to confirm this suggestion and to quantify the importance of higher-order nonlinear effects.

Appendix A: Estimation of Moments of $E_p(f, k, \theta)$

The cross-spectrum $H_{pq}(f)$ of a pair of seafloor pressure sensors, at locations $[x_p, y_p]$ and $[x_q, y_q]$ (Figure 2b), is related to $E_p(f, k, \theta)$ by

$$H_{pq}(f) = \int_0^{k_c} dk \int_0^{2\pi} k\, d\theta \exp\{ik[(x_p - x_q)\cos\theta + (y_p - y_q)\sin\theta]\}E_p(f, k, \theta) \quad \text{(A1)}$$

where k_c is the cutoff wavenumber of waves that reach the seafloor. For small sensor separations, (A1) can be approximated by a truncated expansion:

$$H_{pq}(f) \approx \sum_{n=0}^{N}\sum_{m=0}^{n} i^n \frac{(x_p - x_q)^{n-m}(y_p - y_q)^m}{(n-m)!m!} \cdot \int_0^{k_c} dk \int_0^{2\pi} k\, d\theta\, k^n \cos^{n-m}\theta \sin^m\theta E_p(f, k, \theta) \quad \text{(A2)}$$

where N is the truncation order.

Estimates of moments of $E_p(f, k, \theta)$ (e.g., equations (3) and (4)) are obtained from linear combinations of the normalized cross-spectra

$$\sum_{p,q} \alpha_{pq} \frac{H_{pq}(f)}{[H_{pp}(f)H_{qq}(f)]^{1/2}} \approx \sum_{n=0}^{N}\sum_{m=0}^{n} \beta_{nm} \cdot \frac{\int_0^{k_c} dk \int_0^{2\pi} k\, d\theta\, k^n \cos^{n-m}\theta \sin^m\theta E_p(f, k, \theta)}{\int_0^{k_c} dk \int_0^{2\pi} k\, d\theta\, E_p(f, k, \theta)} \quad \text{(A3)}$$

where the coefficients β_{nm} are given by (A2)

$$\beta_{nm} = \sum_{p,q} \alpha_{pq} i^n \frac{(x_p - x_q)^{n-m}(y_p - y_q)^m}{(n-m)!m!} \quad \text{(A4)}$$

For example, an estimate of $k_{\text{rms}}(f)$ (Eq. 3) can be obtained by choosing weights α_{pq} such that β_{20} and β_{22} are approximately equal to 1 and all other β_{nm} are small (equation (A3)).

Estimates of $k_{\text{rms}}(f)$ (equation (3)) and $\theta_{\text{mean}}(f)$ (equation (4)) based on equations (A3) and (A4) were obtained analytically for a simple six-element array geometry by *Herbers and Guza* [1992]. The estimates presented in this paper were obtained with a more general numerical least squares fit algorithm for arbitrary array geometries described by T. H. C. Herbers, et al. (manuscript in preparation, 1994). Differences between estimates obtained with the analytical and numerical techniques are small.

Appendix B: Bispectra of Weakly Nonlinear Waves

The (third order) seafloor pressure bispectrum $B(f_1, f_2)$ is defined analogous to the conventional (second order) energy density spectrum [*Hasselmann et al.*, 1963]

$$B(f_1, f_2)df_1df_2 = 2\mathbf{E}\{dP(f_1)dP(f_2)dP(-f_1 - f_2)\} \quad \text{(B1)}$$

where $\mathbf{E}\{\ \}$ denotes the expected value and $dP(f)$ is the Fourier-Stieltjes representation of the pressure time series $p(t)$

$$p(t) = \int_{-\infty}^{\infty} dP(f)\ \exp\ (2\pi ift) \quad \text{(B2)}$$

From symmetry considerations the bispectrum is unique only for the domain $f_1 \geq f_2 > 0$.

For weakly nonlinear surface waves, $dP(f)$ can be expressed as

$$dP(f) = \sum_{n=1}^{\infty} dP_n(f) \quad \text{(B3)}$$

with $dP_1(f)$ the lowest order ($O(\varepsilon)$, with ε the perturbation parameter) free wave pressure and $dP_n(f)$ the $O(\varepsilon^n)$ pressure due to forced waves excited by nonlinear interactions of n free wave components [*Hasselmann*, 1962]. Substitution of (B3) in (B1) yields

$$B(f_1, f_2)df_1df_2 = 2\sum_{l=1}^{\infty}\sum_{m=1}^{\infty}\sum_{n=1}^{\infty}\mathbf{E}\{dP_l(f_1)dP_m(f_2)dP_n(-f_1 - f_2)\} \quad \text{(B4)}$$

Assuming the free wave field is Gaussian, the lowest-order ($O(\varepsilon^3)$) term in (B4) $\mathbf{E}\{dP_1(f_1)dP_1(f_2)dP_1(-f_1 - f_2)\}$ vanishes, as do all other odd-order ($n + m + l = 5, 7, \cdots$) terms [*Hasselmann et al.*, 1963]. Keeping sum-frequency interactions only, (B4) reduces to

$$B(f_1, f_2) = \sum_{n=2}^{\infty} B_{2n}(f_1, f_2) \quad \text{(B5)}$$

with B_{2n} the $O(\varepsilon^{2n})$ contribution

$$B_{2n}(f_1, f_2)df_1df_2 = 2\sum_{m=1}^{n-1}\mathbf{E}\{dP_{n-m}(f_1)dP_m(f_2)dP_n(-f_1 - f_2)\} \quad \text{(B6)}$$

The lowest-order (ε^4) term

$$B_4(f_1, f_2)df_1df_2 = 2\mathbf{E}\{dP_1(f_1)dP_1(f_2)dP_2(-f_1 - f_2)\} \quad \text{(B7)}$$

results from phase-coupled triads of two primary wave components with frequencies f_1 and f_2 and the corresponding secondary wave with the sum frequency $f_1 + f_2$. For example, if the primary wave spectrum is narrow with peak frequency f_p, phase-coupled secondary waves with double the peak frequency $2f_p$ excited by (f_p, f_p) interactions yield a nonzero value of $B(f_p, f_p)$.

At the next nonvanishing order (ε^6) the bispectrum contains two terms

$$B_6(f_1, f_2)df_1df_2 = 2[\mathbf{E}\{dP_2(f_1)dP_1(f_2)dP_3(-f_1 - f_2)\} + \mathbf{E}\{dP_1(f_1)dP_2(f_2)dP_3(-f_1 - f_2)\}] \quad \text{(B8)}$$

owing to products of a primary, a secondary, and a tertiary wave component. For a narrow spectrum, phase coupling between the dominant primary (f_p), secondary ($2f_p$, excited by (f_p, f_p) interactions), and tertiary ($3f_p$, excited by (f_p, f_p, f_p) interactions) waves yields a nonzero value of $B(2f_p, f_p)$. Similarly, at the next nonvanishing order (ε^8),

$$B_8(f_1, f_2)df_1df_2 = 2[\mathbf{E}\{dP_3(f_1)dP_1(f_2)dP_4(-f_1 - f_2)\} + \mathbf{E}\{dP_2(f_1)dP_2(f_2)dP_4(-f_1 - f_2)\} + \mathbf{E}\{dP_1(f_1)dP_3(f_2)dP_4(-f_1 - f_2)\}] \quad \text{(B9)}$$

phase coupling between a primary, a tertiary, and a quartenary wave with frequencies f_p, $3f_p$, and $4f_p$, respectively, yields a nonzero value of $B(3f_p, f_p)$, and phase coupling between two secondary waves and a quartenary wave with frequencies $2f_p$ and $4f_p$, respectively, yields a nonzero value of $B(2f_p, 2f_p)$. In general for a narrow spectrum, phase coupling between the first n harmonics with frequencies f_p, $2f_p, \cdots, nf_p$ is expected to contribute to the bispectrum at frequencies $f_1 = (n - m)f_p$, $f_2 = mf_p$ (with $m = 1, 2, \cdots$) (equation (B6)). However, spectra of naturally occurring surface waves are usually broad resulting in a broad bispectrum (e.g., Figures 10 and 12) that cannot be unambiguously interpreted.

Acknowledgments. Support was provided by the Office of Naval Research through the Geology & Geophysics program, the Coastal Sciences program, and the Nonlinear Ocean Waves Accelerated Research Initiative. The pressure array, designed for a 1-month deployment, functioned for 9 months before data acquisition was discontinued. The array was engineered, deployed, and maintained by staff from the Center for Coastal Studies, Scripps Institution of Oceanography. Excellent logistics support was provided by the staff of the U.S. Army Corps of Engineers Field Research Facility, Coastal Engineering Research Center, Duck, North Carolina. J. Redwing generously provided local wind data and helpful suggestions that improved the manuscript. S. Elgar and J. Oltman-Shay made valuable contributions to this field program.

References

Brekhovskikh, L. M., Underwater sound generated by surface waves in the ocean, *Izv. Acad. Sci. USSR Atmos. Oceanic Phys.*, Engl. Transl., *2*, 582–587, 1966.

Cooper, R. I. B., and M. S. Longuet-Higgins, An experimental study of the pressure variations in standing water waves, *Proc. R. Soc. London, Ser. A*, *206*, 424–435, 1951.

Cox, C. S., and D. C. Jacobs, Cartesian diver observations of double frequency pressure fluctuations in the upper levels of the ocean, *Geophys. Res. Lett.*, *16*(8), 807–810, 1989.

Donelan, M. A., J. Hamilton, and W. H. Hui, Directional spectra of wind-generated waves, *Philos. Trans. R. Soc. London, Ser. A*, *315*, 509–562, 1985.

Elgar, S., and R. T. Guza, Observations of bispectra of shoaling surface gravity waves, *J. Fluid Mech.*, *161*, 425–448, 1985.

Hasselmann, D. E., M. Dunckel, and J. A. Ewing, Directional wave spectra observed during JONSWAP 1973, *J. Phys. Oceanogr.*, *10*, 1264–1280, 1980.

Hasselmann, K., On the non-linear energy transfer in a gravity-wave spectrum, Part 1, General theory, *J. Fluid Mech.*, *12*, 481–500, 1962.

Hasselmann, K., A statistical analysis of the generation of microseisms, *Rev. Geophys.*, *1*(2), 177–210, 1963.

Hasselmann, K., et al., Measurements of wind wave growth and swell decay during the Joint North Sea Wave Project (JONSWAP), *Dtsch. Hydrogr. Z.*, suppl. A8, no. 12, 95 pp., 1973.

Hasselmann, K., W. Munk, and G. MacDonald, Bispectra of ocean waves, in *Times Series Analysis*, edited by M. Rosenblatt, pp. 125–139, John Wiley, New York, 1963.

Haubrich, R. A., Earth noise, 5 to 500 millicycles per second, 1, Spectral stationarity, normality, and nonlinearity, *J. Geophys. Res.*, *70*(6), 1415–1427, 1965.

Haubrich, R. A., W. H. Munk, and F. E. Snodgrass, Comparative spectra of microseisms and swell, *Bull. Seismol. Soc. Am.*, *53*(1), 27–37, 1963.

Herbers, T. H. C., and R. T. Guza, Estimation of directional wave spectra from multicomponent observations, *J. Phys. Oceanogr.*, *20*(11), 1703–1724, 1990.

Herbers, T. H. C., and R. T. Guza, Wind-wave nonlinearity observed at the sea floor, Part 1, Forced wave energy, *J. Phys. Oceanogr.*, *21*(12), 1740–1761, 1991.

Herbers, T. H. C., and R. T. Guza, Wind-wave nonlinearity observed at the sea floor, Part 2, Wavenumbers and third order statistics, *J. Phys. Oceanogr.*, *22*(5), 489–504, 1992.

Herbers, T. H. C., S. Elgar, and R. T. Guza, Infragravity-frequency (0.005–0.05 Hz) motions on the shelf, Part 1, Forced waves, *J. Phys. Oceanogr.*, *24*(5), 917–927, 1994.

Herbers, T. H. C., R. L. Lowe, and R. T. Guza, Field observations of orbital velocities and pressure in weakly nonlinear surface gravity waves, *J. Fluid Mech.*, *245*, 413–435, 1992.

Hughes, B., Estimates of underwater sound (and infra sound) produced by non-linearly interacting ocean waves, *J. Acoust. Soc. Am.*, *60*(3), 1032–1039, 1976.

Kibblewhite, A. C., and K. C. Ewans, Wave-wave interactions, microseisms, and infrasonic ambient noise in the ocean, *J. Acoust. Soc. Am.*, *78*(3), 981–994, 1985.

Kibblewhite, A. C., and C. Y. Wu, The generation of infrasonic ambient noise in the ocean by non-linear interactions of ocean surface waves, *J. Acoust. Soc. Am.*, *85*(5), 1935–1945, 1989.

Kibblewhite, A. C., and C. Y. Wu, The theoretical description of wave-wave interactions as a noise source in the ocean, *J. Acoust. Soc. Am.*, *89*(5), 2241–2252, 1991.

Leffler, M. W., C. F. Baron, B. L. Scarborough, K. K. Hathaway, and R. T. Hayes, Annual data summary for 1990, *Tech. Rep. CERC-92-3*, Coastal Eng. Res. Cent. Field Res. Facil., U.S. Army Corps of Eng. Waterways Exp. Sta., Vicksburg, Miss., 1992.

Leffler, M. W., C. F. Baron, B. L. Scarborough, and K. K. Hathaway, Annual data summary for 1991, technical report, Coastal Eng. Res. Cent. Field Res. Facil., U.S. Army Corps of Eng. Waterways Exp. Sta., Vicksburg, Miss., in press, 1994.

Longuet-Higgins, M. S., A theory of the origin of microseisms, *Philos. Trans. R. Soc. London, Ser. A*, *243*, 1–35, 1950.

Longuet-Higgins, M. S., and F. Ursell, Sea waves and microseisms, *Nature*, *162*, 700, 1948.

Longuet-Higgins, M. S., D. E. Cartwright, and N. D. Smith, Observations of the directional spectrum of sea waves using the motions of a floating buoy, in *Ocean Wave Spectra*, pp. 111–136, Prentice-Hall, Englewood Cliffs, N. J., 1963.

Masuda, A., and Y.-Y. Kuo, Bispectra for the surface displacement of random gravity waves in deep water, *Deep Sea Res., Part A*, *28*(3), 223–237, 1981.

Miche, M., Movements ondulatoires de la mer en profondeur constante ou decroissante, *Ann. Ponts Chaussees*, *114*, 25–87, 131–164, 270–292, 396–406, 1944.

Mitsuyasu, H., F. Tasai, T. Suhara, S. Mizuno, M. Ohkusu, T. Honda, and K. Rikiishi, Observations of the directional spectrum of ocean waves using a cloverleaf buoy, *J. Phys. Oceanogr.*, *5*, 750–760, 1975.

Nichols, R. H., Infrasonic ambient ocean noise measurements: Eleuthera, *J. Acoust. Soc. Am.*, *69*, 974–981, 1981.

Phillips, O. M., On the dynamics of unsteady gravity waves of finite amplitude, Part 1, The elementary interactions, *J. Fluid Mech.*, *9*, 193–217, 1960.

Tyler, G. L., C. C. Teague, R. H. Stewart, A. M. Peterson, W. H. Munk, and J. W. Joy, Wave directional spectra from synthetic aperture observations of radio scatter, *Deep Sea Res.*, *21*, 989–1016, 1974.

Webb, S. C., and C. S. Cox, Observations and modeling of seafloor microseisms, *J. Geophys. Res.*, *91*(B7), 7343–7358, 1986.

Yamamoto, T., and T. Nye, A hundred-day observation of microseism evolution in shallow water using a 6-point shallow buried OBS/P array, *J. Acoust. Soc. Am.*, *91*(4), 2345, 1992.

R. T. Guza, Center for Coastal Studies, 0209, Scripps Institution of Oceanography, La Jolla, CA 92093-0209.

T. H. C. Herbers, Department of Oceanography, Naval Postgraduate School, Monterey, CA 93943-5000.

(Received May 20, 1993; revised November 30, 1993; accepted December 8, 1993.)